Materials & Design 223 (2022) 111263

Contents lists available at ScienceDirect

Materials & Design

journal homepage: www.elsevier.com/locate/matdes

Rapid and ultrasensitive detection of SARS-CoV-2 spike protein based on upconversion luminescence biosensor for COVID-19 point-of-care diagnostics

Lihua Li [a], Menglin Song [a], Xinyue Lao [a], Sin-Yi Pang [a], Yuan Liu [a], Man-Chung Wong [a], Yingjin Ma [a], Mo Yang [b], Jianhua Hao [a,*]

[a] Department of Applied Physics, The Hong Kong Polytechnic University, Hung Hom, Kowloon, Hong Kong, China
[b] Department of Biomedical Engineering, The Hong Kong Polytechnic University, Hung Hom, Kowloon, Hong Kong, China

HIGHLIGHTS

- Highly sensitive and rapid detection of spike protein was constructed based on FRET effect.
- The detection in the NIR region is sensitive and specific and the mechanism was illustrated.
- The detection system could satisfy S protein and nucleocapsid protein detection simultaneously.

GRAPHICAL ABSTRACT

We developed a novel nanosystem composed of UCNPs and Au nanorods for capturing and detecting S protein based on the Förster resonance energy transfer fluorescence (FRET) effect.

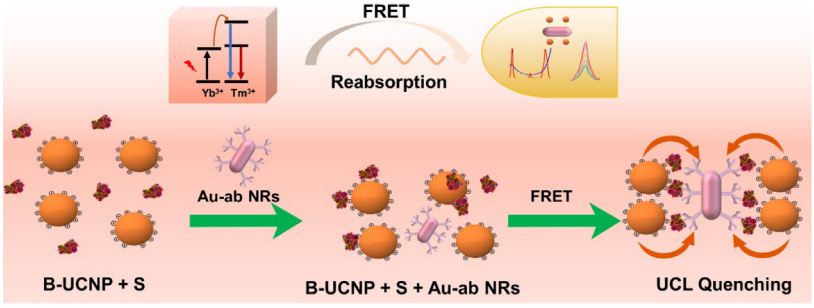

ARTICLE INFO

Article history:
Received 23 September 2022
Revised 7 October 2022
Accepted 16 October 2022
Available online 17 October 2022

Keywords:
Upconversion nanoparticles
Au nanorods
COVID-19 point-of-care diagnostics
FRET effect
SARS-CoV-2 spike protein

ABSTRACT

Here, we firstly introduce a detection system consisting of upconversion nanoparticles (UCNPs) and Au nanorods (AuNRs) for an ultrasensitive, rapid, quantitative and on-site detection of SARS-CoV-2 spike (S) protein based on Förster resonance energy transfer (FRET) effect. Briefly, the UCNPs capture the S protein of lysed SARS-CoV-2 in the swabs and subsequently they are bound with the anti-S antibodies modified AuNRs, resulting in significant nonradiative transitions from UCNPs (donors) to AuNRs (acceptors) at 480 nm and 800 nm, respectively. Notably, the specific recognition and quantitation of S protein can be realized in minutes at 800 nm because of the low autofluorescence and high Yb-Tm energy transfer in upconversion process. Inspiringly, the limit of detection (LOD) of the S protein can reach down to 1.06 fg mL^{-1}, while the recognition of nucleocapsid protein is also comparable with a commercial test kit in a shorter time (only 5 min). The established strategy is technically superior to those reported point-of-care biosensors in terms of detection time, cost, and sensitivity, which paves a new avenue for future on-site rapid viral screening and point-of-care diagnostics.

1. Introduction

Coronavirus disease 2019 (COVID-19), caused by severe acute respiratory syndrome coronavirus 2 (SARS-CoV-2), is the most sig-

* Corresponding author.
E-mail address: jh.hao@polyu.edu.hk (J. Hao).

https://doi.org/10.1016/j.matdes.2022.111263
0264-1275/

nificant pandemic around the world today and brought a terrific threat to human beings [1]. Until now, COVID-19 has undergone several variations, which infected more than 577 million people and directly caused 6.40 million deaths globally. The pandemic remains volatile and is challenging to prevent. Especially, asymptomatic infected individuals of all ages can still transmit the virus to others[2]. Containment measures including on-site and sensitive detection of COVID-19 are an urgent key to protecting health and preventing the spread of the pandemic. The official and gold standard for detecting SARS-CoV-2 approach is reverse transcription-polymerase chain reaction (RT-PCR) [3]. However, it takes hours, and needs expensive agents and equipment, as well as professionals. Thus, great attention and efforts have been paid to developing rapid SARS-CoV-2 detection using various methods[4,5], such as the enzyme-linked immunoassay method (ELISA), colloidal gold method[6], optical biosensors[7], and microfluidic detection[8]. The specific proteins (spike protein[9], membrane protein, and nucleocapsid protein[10]) and protease[11] expressed in SARS-CoV-2 have emerged as candidate biomarkers, which provide alternative approaches for implementing preventive measures. Especially, the spike (S) proteins have gained considerable interest in SARS-CoV-2 study owing to their distinct features, including that they are highly expressed on the surface of SARS-CoV-2 and responsible for binding as well as entering into the host cells[12]. S proteins are the primary antigens in infection and possess a more stable protein structure [13]. Therefore, by virtue of the functional effects and structural importance of S protein in SARS-CoV-2, it is selected as the optimal target analyte for live COVID-19 detection in this work.

On the other hand, upconversion nanoparticles (UCNPs) have the merits of chemically stable, large anti-Stokes shifts, low background noises, tunable size, and resistance to photobleaching[14–16], which confer them significant superiority in various biosystem detection, such as protein, microRNA, DNA, metal ions and bacteria [17–19]. A novel mechanism of UCNP-based bio-detection system is the changes in Förster resonance energy transfer (FRET) efficiency caused by the donor (UCNP) and energy acceptor after the addition of the target analytes[20]. The energy transfer in FRET is an intermolecular dipole–dipole coupling, i.e., a very close distance (1–10 nm) from donor to acceptor[7]. And the donor emission spectra should be overlapped with the absorption spectra of the acceptor molecule to ensure the non-radiative transition. Thus, the FRET-based detection is affected by two essential factors, i) the overlap of absorption spectra of the acceptor and emission spectra of the donor; ii) the size of the analyst corresponding to the distance between the donor and acceptor. In particular, the biomolecules, polypeptides, and proteins match well with the distance and thus the UCNP-based luminescence platform has gained great merits in the detection of biomolecules and live organisms. Unfortunately, there are currently no reports on UCNPs-based nanoprobe for the detection of S protein in SARS-CoV-2.

Inspired by the exclusive optical features of UCNPs and AuNRs. Here, we developed an ultrarapid, sensitive, and on-site detection of SARS-CoV-2 S protein based on the FRET effect between UCNPs and AuNRs. The main advantages of this work include (i) the high positive UCNPs are capable of capturing the free S protein efficiently, ensuring that the linker between energy excitation donor and acceptor is short enough to afford resonance between their excited states. Subsequently they are combined with the anti-spike antibody functionalized AuNRs (Au-ab), thus resulting in a high energy transfer efficiency between UCNPs and AuNRs; (ii) Since conventional UCNPs-based FRET biosensors are potentially susceptible to interference with the auto-fluorescence and irrelevant protein pollutants in the samples in visible region resulting in false-positive results, the detection peak in the near-infrared (NIR) region (800 nm) in this work illustrates a high and specific luminescence response with negligible background interference from the sample because of the low autofluorescence and high Yb-Tm energy transfer at 800 nm. In particular, the established assay needs fewer reagents, and it could be completed in minutes with the limit of detection (LOD) of S protein as low as 1.06 fg mL^{-1} and normal recognition of nucleocapsid protein (comparable with commercial test kit). It is promising that the established nanoprobes could realize the ultrarapid, high sensitivity, and on-site detection of SARS-CoV-2 surface antigens. More importantly, this design provides a new way of UCNP-based protein assay, which can be potentially expanded to the detection of related antigens, antibodies and proteins.

2. Materials of methods

2.1. Materials

SARS-CoV-2 Spike protein (RBD, His & Avi tag), SARS-CoV-2 Spike S1 antibody were purchased from GeneScript (USA). Ethylene glycol (EG, 99 %), Branched polyethyleneimine (PEI, 25 kDa), NaCl (99 %), $Y(NO_3)_3{\cdot}6H_2O$, $Yb(NO_3)_3{\cdot}5H_2O$, $Tm(NO_3)_3{\cdot}6H_2O$ were purchased from Aladdin (China) and used as agents without further purification.

2.2. Synthesis of $NaYF_4$:Yb/Tm

The UCNPs were fabricated via a typical hydrothermal method with slightly modification[21]. Briefly, NaCl (1.2 mmol) was firstly added to 9 mL EG and agitated until a transparent solution formed, $Y(NO_3)_3{\cdot}6H_2O$ (0.48 mmol), $Yb(NO_3)_3{\cdot}5H_2O$ (0.119 mmol), $Tm(NO_3)_3{\cdot}6H_2O$ (0.001 mmol), and PEI (0.2 g) was added to the above solution with fierce stirring for 30 min. NH_4F (3.3 mmol) dissolved in 6 mL EG was added to the mixture and agitated for another 15 min. Then the resulting mixture was transferred to a 20 mL Teflon-lined autoclave and heated at 190 °C for 2 h. The obtained UCNPs were separated using acetone as precipitator and collected by centrifugation, washed with ethanol and DI water for several times.

2.3. Fabrication of Ligand-free UCNPs

To remove the abundant PEI on the surface of UCNPs, 60 mg UCNPs were dissolved in 15 mL ethanol with 112 μL HCl (36 wt %) under sonication for 30 min, then the solution was centrifuged at 7000 rpm for 5 min to remove the supernatant. The UCNPs were purified using ethanol and dried for further use[22].

2.4. Preparation of AuNRs

The AuNRs were synthesized using a previous method[23]. Typically, seed solution and growth solution were fabricated as below,

Seed solution. 1 mL CTAB solution (0.2 M) and 1 mL $HAuCl_4$ solution (0.5 mM), after vigorously stirring, 0.2 mL $NaBH_4$ (0.006 M) was added to the solution and agitated at 1400 rpm for 2 min, a brownish yellow solution was formed and aged for 30 min for further use.

Growth solution. 0.7 g CTAB (3.7 mM) and 0.1234 g NaOL (4.7 mM) were dissolved in 25 mL distilled water with vigorously stirring at 50 °C, the solution was kept at 25 °C after totally dissolution. Subsequently, 2.4 mL $AgNO_3$ (4 mM) was added to the above solution and kept undisturbed for another 15 min. 25 mL $HAuCl_4$ (1 mM) was added to the mixture, and the solution changed from golden to colorless at 90 min. Then 0.15 mL concentrated HCl was added to the solution and agitated slowly for another

15 min. 0.125 mL ascorbic acid (64 mM) added to the solution and stirring at 1500 rpm for 30 s. Finally, 40 μL seed solution was added to the growth solution, and the mixture was stirring vigorously for 30 s and kept still for 12 h at 30 °C. The AuNRs were separated by centrifuging at 7000 rpm for 30 min.

2.5. Thiolated of anti-SARS-COV19 IgM[24]

0.1 mL of anti-SARS-COV19 Immunoglobulin M (IgM, 0.1 mg mL^{-1}) was dissolved in Buph PBS (0.1 M PBS containing 10 mM EDTA). Subsequently, 5 μL DTT (1 M) in Buph PBS were added to the above solution and stirring at 37 °C for 2 h. To remove the abundant DTT, the solution was flushed the Nap-5 column[25].

2.6. Functionalization of AuNRs with thiolated antibodies

Briefly, 10, 50, and 100 μL of thiolated anti-SARS-COV19 IgM (100 μg/mL) was added dropwise to 1 mL of AuNR solution, respectively. In detail, there was $\sim 1.2 \times 10^{11}$ antibodies in every 10 μL antibody, and the concentration of AuNRs is calculated to be $\sim 1 \times 10^{11}$ in the reaction solution. After stirring for 30 min, 150 μL Methoxy-PEG-SH (PEG-SH) (1 M) was added by drop to the above solution and kept stirring for 2 h at room temperature, the excess PEG-SH was removed by centrifugation colloidal solution after 5 min of GNRs and anti-IgG incubation at room temperature with stirring, which was then kept for 2 h. The optimal concentration of IgM modified Au-IgG NPs were selected by the sensitivity.

2.7. The UCL quenching

B-UCNPs were firstly incubated with S protein of different concentrations (0, 2, 4, 8, 16, 32, 100, 1000 fg mL^{-1}), and Au-ab NRs were added to the solutions and incubated for different time intervals (5, 30, 60, 90 min), the photoluminescence spectra were recorded using Edinburgh analytical instrument under 980 nm laser excitation. The photoluminescence intensity was repeated for 3 individual experiments at each concentration.

The UCL quenching efficiency was calculated as below,

$$Q_e\% = 100 - \frac{Q_s}{Q_c} \times 100 \quad (1)$$

where Qs and Qc are the upconversion luminescence of samples + UCNP and UCNP.

2.8. Sample detection

Different concentrations of S protein (1, 2, 4, 8, 16 fg mL^{-1}) were added to simulant saliva and swab, respectively. After lysis for 2 min, the samples were tested using the fabricated UCNP-Au nanoprobes. The results were compared with the standard curve. The Qe was calculated as equation (1).

The detection of limit (LOD) was calculated as below:

$$\mathrm{LOD} = \frac{3Sa}{b} \quad (2)$$

Where *Sa* is the standard deviation of the response and b is the slope of the calibration curve.[26].

2.9. The effect of interferants in detection

PBS, lysis buffer, ddH_2O and swabs added to the nanosystem to evaluate their effect on the detection system, their emission wavelength from 450 to 850 nm was measured using FLSP920 Edinburgh analytical instrument. In addition, gradient concentrations of human serum albumin (HSA) (0.1, 0.2, 0.4, 0.8, 1.6 mg mL^{-1}) and sialic acid (SA) (0.1, 0.2, 0.4, 0.8, 1.6 mg mL^{-1}) were also added to the detection system, respectively, and their emission wavelength were recorded. The photoluminescence intensity at 480 nm and 800 nm was averaged by the data repeated for five times.

2.10. Detection of S protein in swab

Different concentrations (1, 2, 4, 8, 16 fg mL^{-1}) of S protein were added to swabs, their emission wavelength were recorded and the Qe at 480 nm and 800 nm were calculated respectively. In blind samples, 2.5, 3.0, 4.5, 5.0, 6.0, 7.5, 8.0, 10.5, and12 fg S protein were added randomly to the swabs, and the samples were detected at 800 nm to calculate their contents.

2.11. Detection of nucleocapsid protein

Gradient concentrations (6.25, 12.5, 25, 50, 100 pg mL^{-1}) of nucleocapsid protein were tested in the nanosystems, their Qe at 480 nm and 800 nm were calculated. In addition, 200 μL 25, 50, 100 pg mL^{-1} and 1 ng mL^{-1} nucleocapsid protein were also tested using the commercial kits (COVID-19 Ag Test Kit), which work as reference.

3. Results and discussions

3.1. Design of FRET-based S protein detection nanoprobe

The design and scheme of the detection is illustrated in Scheme 1, in which AuNR-UCNP assemblies are designed to detect S protein with ultralow LOD (1.06 fg mL^{-1}). The formed core-satellite geometric structure of AuNR-UCNP assemblies makes the ultrasensitive detection possible because of the quick combination of UCNPs and AuNRs and the strong resonance between the excited states of UCNPs and AuNRs. Briefly, the swabs containing SARS-CoV-2 are lysed in lysis buffer, the mixture containing negative S protein is firstly co-cultured with the bare UCNPs (B-UCNP, with high positive potential), and a protein "corona" is formed on the surface of B-UCNPs due to the electrostatic attraction. Subsequently, the B-UCNPs with S protein are specifically attached to the Au-ab NRs, forming an orderly rearrangement of B-UNCPs around Au-ab NRs. Thus, an enhanced and concentration-dependent FRET process between UCNPs and AuNRs occurs, which induces a significant fluorescence quenching of UCNPs. Moreover, the acid-treated UCNPs may cause a redistribution of Tm on the surface of UCNPs[27] and exhibit high FRET efficiency, leading to ultra-sensitive detection of S protein.

3.2. Characterizations of UCNPs and AuNRs

The monodisperse $NaYF_4$:Yb/Tm NPs were synthesized by a one-step hydrothermal method. Branched PEI was employed as ligand and surfactant to control the size, growth, and photoluminescence (PL) of the UCNPs[18]. As could be seen in Fig. 1, the PEI-$NaYF_4$:Yb/Tm NPs exhibit excellent water dispersity, with an average size of 30 ± 2 nm. X-ray diffraction (XRD) spectrum in Fig. S1 illustrates that the peaks in PEI-$NaYF_4$:Yb/Tm correspond well with the standard cubic $NaYF_4$ NPs (JCPDS 77-2042). Moreover, the high-resolution STEM image (Fig. 1b) is in accordance with the (111) main plane of XRD results, confirming the cubic structure of PEI-$NaYF_4$:Yb/Tm. Elemental mapping (Fig. 1c) further illustrates the elemental compositions of Y, Yb, and Tm in UCNPs. The PEI on the surface endows the UCNPs with high dispersity and zeta potential (+37 mV, Fig. S2). On the other hand, the prepared UCNPs with PEI coatings may reduce those emitting ions

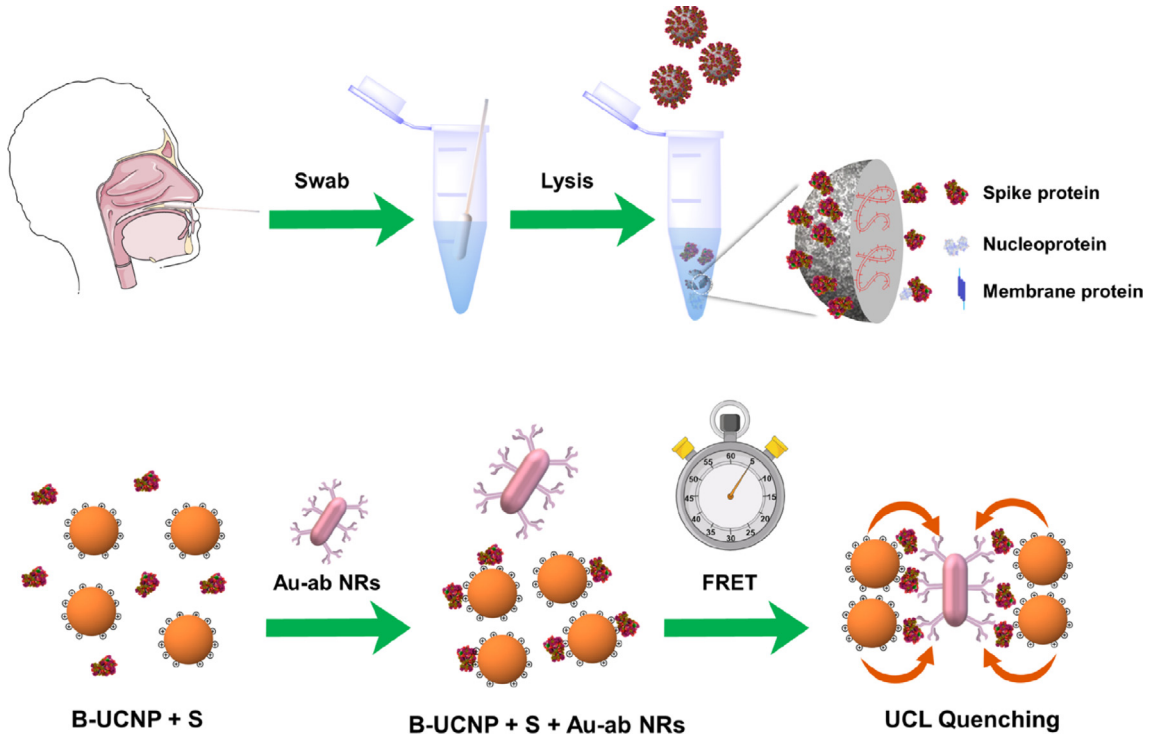

Scheme 1. Schematic illustration of ultrarapid S protein detection using UCNP and AuNR system. The S protein is firstly attached to the surface of UCNPs due to high electrostatic attraction and then captured by the Au-ab NRs. Thus, an energy transfer from donor to acceptor will be occurred, and this FRET effect induces a significant decrease in upconversion luminescence.

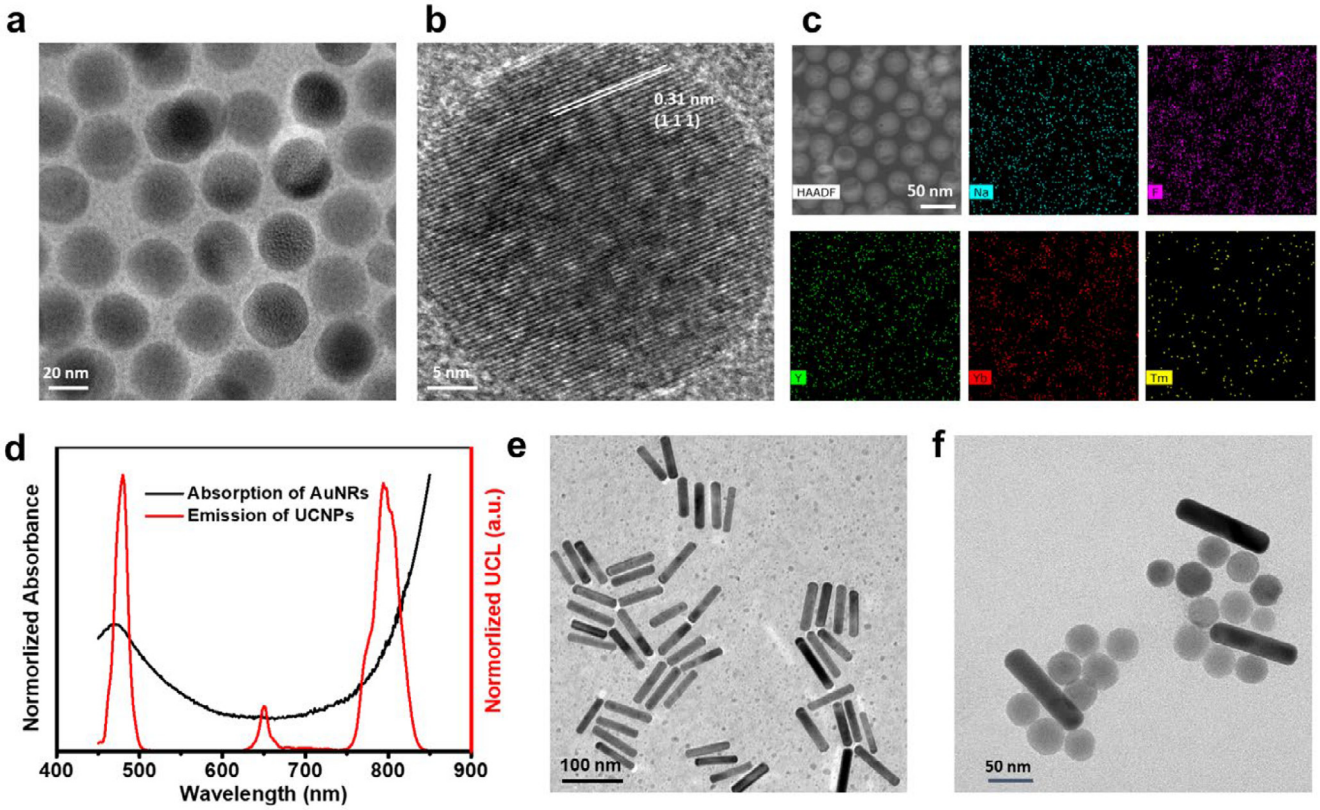

Fig. 1. Characterization of $NaYF_4$:Yb/Tm and AuNRs. a. TEM image of $NaYF_4$:Yb/Tm NPs. **b.** HRTEM image of $NaYF_4$:Yb/Tm. **c.** STEM image and Na, F, Y, Yb and Tm mapping of the NPs. **d.** Fluorescence spectrum of UCNP and absorption spectrum of AuNRs. The emission spectrum of UCNP overlaps well with the absorption spectrum of AuNRs, illustrating a promising FRET effect. The absorption spectrum was normalized at 850 nm. The upconversion luminescence spectrum was normalized at 480 nm. **e.** TEM image of AuNRs. **f.** TEM image of core-satellite structure of AuNRs and UCNPs after addition of target (S protein).

near the surface of NPs and enlarge the distance between donors and acceptors, thus finally limiting the FRET efficiency. Typically, PEI on the surface of UCNPs efficiently enhance their hydrophilic radius[28]. PEI is estimated to be above 100 nm in its free state [29]. Here, we treated PEI-UCNPs with HCl to remove PEI ligand on the surface and the bare UCNPs were prepared, termed as B-UCNPs. Notably, the average sizes measured by dynamic light scattering (DLS) decrease from 45 nm to 30 nm (Fig. S2). The dispersity and crystal form (XRD pattern) of the B-UCNPs remains the same as the original PEI-UCNPs (Fig. S1). Meanwhile, the zeta potential increases to 60 mV (Fig. S3) after acid treatment and a more stable solution is formed. Fourier transform infrared spectroscopy (FTIR) results further confirms the successful removal of PEI on the surface of B-UCNPs (Fig. S4). Thus, most emitting ions are inclined to appear near the surface of the UCNPs and the donors are close to the acceptors. In addition, there is no extra modification on the surface of B-UCNPs, i.e., the donor-to-acceptor distance is minimum (Fig. S2)[30]. Upon the excitation under 980 nm laser, the B-UCNPs exhibited typical Tm^{3+} emission peaks (Fig. 1 d), the emissions at 480 nm and 650 nm are attributed to the energy transitions from $^1G_4$ to $^3H_6$ and $^1G_4$ to $^3F_4$, respectively. And the emission at 800 nm is arisen from the energy transition from $^3H_4$ to $^3H_6$[31]. These main peaks are attributed to blue, red and NIR emissions, which correspond well to the absorption spectra of AuNRs (Fig. 1d). In addition, there is a negligible decrease in upconversion luminescence (UCL) after the removal of PEI ligand (Fig. S5), which is superior to the similar operation on OA-UCNPs [32].

Simultaneously, AuNRs with a length of 78 ± 2 nm and width of 15.5 nm, and the aspect ratio of 5.03 were precisely synthesized (Fig. 1e), the longitudinal absorption of the AuNR is centered at 965 nm (Fig. S6), the absorption spectra overlap well with the emission spectra of the UCNPs (480 nm, 800 nm) and the excitation light (Fig. 1d). Here, AuNRs exhibited a high zeta potential (+38 mV) because of the hexadecyl trimethyl ammonium bromide (CTAB) ligand on their surface (Fig. S2).

3.3. FRET-based spike protein detection

Before further optimization, we firstly test the validity and accuracy of the nanoprobes. AuNRs were modified with thiolated anti-spike antibody (i.e. human IgM in this case) and further blocked with SH-PEG. Here, the covalent bond of antibody and PEG on the surface of AuNRs is stronger than the ionic bond of CTAB. The successful modification is verified by UV–vis (Fig. S6), the additional absorption peak at 260 nm confirms the successful conjunction of antibodies on the surface of AuNRs. Correspondingly, the zeta potential decrease from 32.8 mV to 10 mV after modification of antibody and PEG (Fig. S2). The positive zeta potential keeps the stabilization of Au-ab solution as well as maintains a certain distance from the high positive UCNPs (Fig. S2), ensuring the stability and specificity of the detection system. Notably, AuNR-UCNP satellite structures are formed after addition of S protein (Fig. 1 e). Interestingly, the average distance from UCNP to AuNRs is estimated to be 3.03 ± 0.23 nm according to the TEM images taken from randomly selected locations. It is worth stressing that, the length of S protein at UCNP terminal and antibody at Au surface is larger than the distance in the TEM image because of that their distance has been largely decreased from the dry state-characteristic and the hybridization of antigen–antibody effect in TEM image [33]. In a control group with only AuNRs bearing free antibody, no assemblies of Au-UCNP were formed, the UCNPs and AuNRs are in a far distance (>10 nm) and this random distribution is due to the electrostatic repulsive and capillary forces as well (Fig. S7).

As shown in Fig. 2a, S protein was firstly incubated with B-UCNPs, then Au-ab NRs were added to the solution and AuNR-UCNP clusters were formed *via* antigen–antibody reaction, resulting in a close distance between UCNPs and Au-ab NRs, which leads to the decrease of UCL due to FRET effect. The strong absorption at 980 nm of AuNRs results in the decreased energy and reverse energy transfer to UCNPs, thus finally quenching the luminescence of UCNPs[34] (Fig. 2b). After addition of the target S protein, a specific capture and conjugation of B-UCNP and Au-ab NRs were established, the distance between AuNRs and B-UCNPs decreases significantly *via* the hybridization of antigen and antibody, which further induce a dramatic UCL quenching at the characteristic emission peaks (Fig. 2b). The energy transfer (E_T) efficiency can be expressed as:

$$E_T = \frac{\text{Ic-Is}}{\text{Ic}} \tag{3}$$

I_c and I_s are the UCL intensities of UCNP and UCNP + AuNRs, respectively.

The E_T transfer efficiency (0.51) from UCNP to AuNRs at 800 nm is higher than that (0.45) at 480 nm. In addition, the contribution of Au-ab NRs and S protein in FRET has also been studied using the changes in decay time. As shown in Fig. 2 c and d, there is negligible changes of decay time after adding Au-ab NRs to the B-UCNP nanosystem, illustrating non-FRET effect and reabsorption effect in this process. Interestingly, the decay curves of B-UCNPs, B-UCNPs + Au-abs, and B-UCNPs + S + Au-abs at 480 nm are shown in Fig. 2c, the lifetime is reduced from 0.370 ms to 0.212 ms[35] followed by adding S protein in the nanoprobes, and the phenomena is particularly obvious at 800 nm (Fig. 2d), with a lifetime of 0.559 ms and 0.195 ms. Both the decreased UCL intensity and shortened lifetime prove the close distance between the donors and acceptors, and this further induces a strong nonradiative energy transfer from UCNPs to acceptors, which was in accordance with the TEM result (Fig. 1c) and previous studies[32,36]. Notably, the UCNP-AuNR nanoprobes exhibited a more dramatically decreased in decay time and higher E_T transfer efficiency after addition of S protein at 800 nm compared with 480 nm, illustrating a highly specific and sensitive recognition of target at NIR region.

3.4. Optimization of the detection sensitivity

Antibody amounts on AuNRs and incubation time are two key factors that could affect overall S protein test performance. Firstly, different antibody loading volumes on AuNRs were optimized with the same incubation time (5 min). As shown in Fig. 3, AuNRs with different loading contents of antibody give rise to the observed concentration-dependent responsiveness of S protein, and the UCL intensities at 450–500 nm and 750–850 nm decreased with the increase of S contents because of the FRET effect. The UCL quenching is evident to show a high S protein concentration-dependence among all groups. Fig. 3a, b show no obvious linear trend between S protein and quenching efficiency because of fewer antibodies on the AuNRs (∼1 antibody on AuNR). When the concentration of antibodies on AuNRs increased, the system exhibited high sensitivity toward S protein with a linear relationship against the mass or logarithmic (log) mass between the concentrations from 2 fg mL^{-1} to 32 fg mL^{-1} (Fig. 3 c - f). Notably, when 50 μL 100 μg mL^{-1} of antibody ($\sim 6 \times 10^{11}$) is used, each AuNR bares about 5–6 antibodies ($\sim 1 \times 10^{11}$ AuNRs in the nanoprobe)[37], the group showed the highest sensitivity in 800 nm among all groups with a LOD of 1.06 fg mL^{-1}. The detection results are reproducible and the LOD is calculated by the standard error in response divided by the slope of the linear fitting. When the number of ab on each AuNR reaches up to 8–10, the maximum quenching efficiency reaches 50 %, however, there was no improvement on LOD

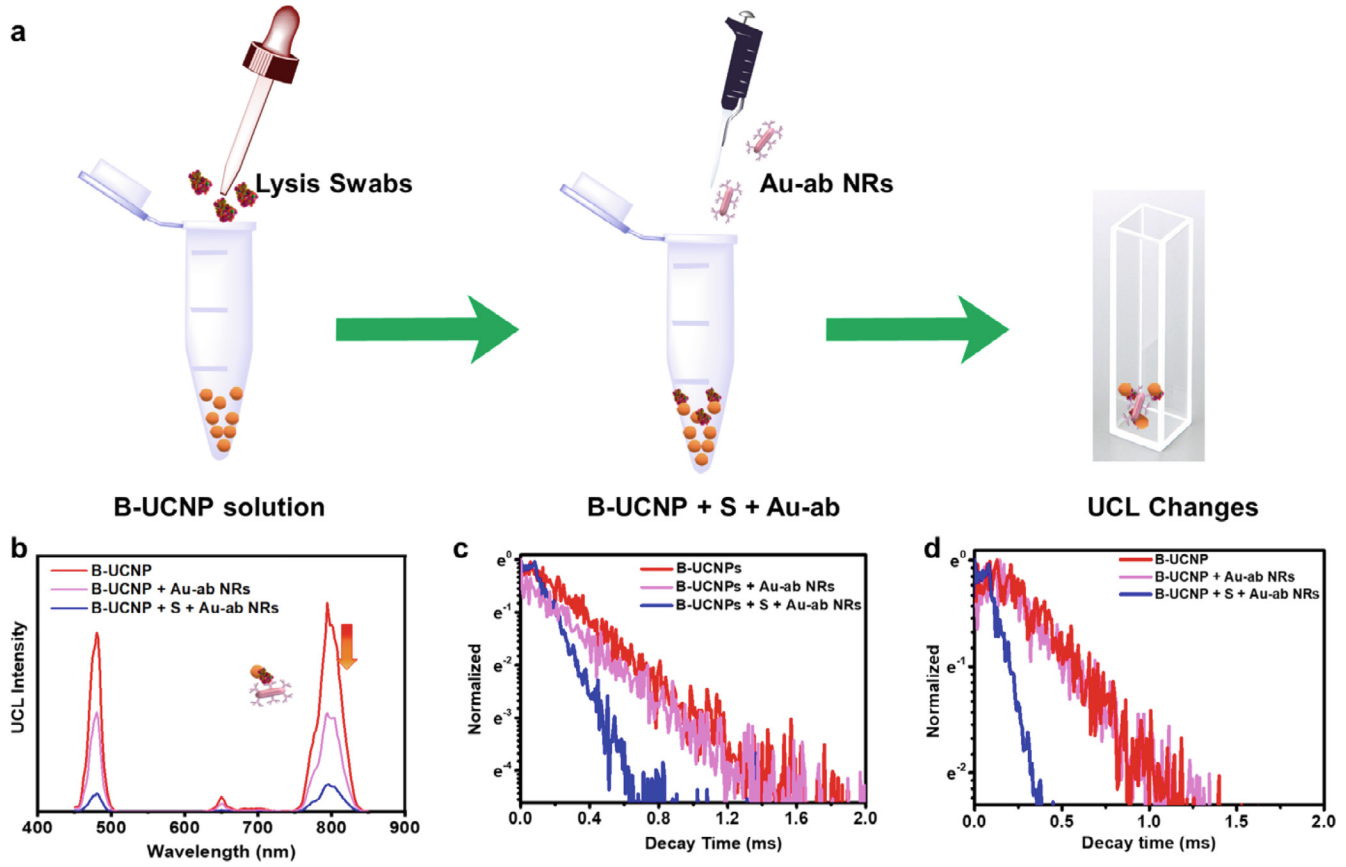

Fig. 2. FRET-based detection of S protein. a. Work flow of ultra-rapid detection of S protein using UCNP and AuNR based biosensors. **b.** UCL changes after addition of Au-ab NRs, and Au-ab NRs with S protein (1 ng mL^{-1}). Lifetime changes after addition of Au-ab NRs, and Au-ab NRs with S protein at **c**. 480 nm, and **d.** 800 nm. The marked lifetime is determined by fitting the PL decay with a single exponential function.

(1.13 fg mL^{-1} at 800 nm). Thus, 5–6 abs were selected as the optimal concentration and this group is selected for the next study. Notably, the detection of S protein at 800 nm (LOD = 1.06 fg mL^{-1}) illustrates a higher sensitivity compared to the detection capability at 480 nm (LOD = 2.68 fg mL^{-1}). The *ET* at 800 nm is 0.40 with the S protein of 32 fg mL^{-1}, which is higher than that at 480 nm (*ET* = 0.38) under identical condition. Therefore, low background, non-autofluorescence, high ET transfer efficiency and ultra-sensitivity endow the incomparable merits for S protein detection at the NIR region. The UCL changes at 650 nm have also been investigated, further studies in this region are excluded due to the weak and irregular changes. In addition, we also assess the effectiveness of B-UCNP and Au system on S protein detection, there are no obvious changes of UCL intensity after addition of different concentrations of S protein (Fig. S8), which are consistent with the above TEM image (Fig. S7). Therefore, the proper antibodies on AuNRs and selected detection region can improve the sensitivity and enhance the FRET effect[9].

The incubation time is highly related to the convenience and practicability of real sample detection, here, we optimized the incubation time with 5 min (data in Fig. 3), 30 min, 60 min and 90 min. The results are shown in Fig. 4, there are significant UCL quenching measured in the wavelength of 480 nm and 800 nm after addition of S protein at all incubation intervals. Importantly, the sensing S protein enjoys a linear response with the UCL quenching at 800 nm emission from 1 fg mL^{-1} to 16 fg mL^{-1} at all time intervals. Briefly, the relationship between quenching efficiency and concentration is shown in the inset of Fig. 4 b after incubation for 30 min, fitted as $y = 22.75\log_{10}x + 2.927$. When incubated for 60 min, the quenching efficiency exhibits an excellent linear response to S protein concentration (1–16 fg mL^{-1}) at 480 nm and 800 nm, the linear relationships are depicted as $y = 53.37\log_{10}x + 16.8$ and $y = 43.65\log_{10}x - 0.06$ at 480 nm and 800 nm, respectively. When the cocultured time increase to 90 min, conjugating S protein shows dramatical influence on UCL quenching, the UCL quenching efficiency is able to reach up to 95 % and 87 % at 480 nm and 800 nm, respectively. In addition, the quenching efficiency soon reach the upper at 480 nm after co-cultured for 90 min with 4 fg mL^{-1} of S protein. By contrast, there is still an unsaturated magnitude at 800 nm at 100 fg mL^{-1}, which means a wide detection range of S protein in NIR region. The results further illustrate the reliability and feasibility of S protein detection at 800 nm. PEI-UCNPs have also been applied as biosensors under the similar condition for comparison. At the optimized condition (90 min, 5 ~ 6 antibodies on AuNRs), the quenching efficiency on PEI-UCNP is significantly lower than B-UCNPs and the sensitivity is dramatically reduced (Fig. S9). The result further demonstrates the merits of B-UCNPs in S detection. And the main reasons may be that more Ln^{3+} ions are apt to occupy on the surface of the particles during the HCl treated process, thus resulting in an efficient FRET. By contrast, PEI-UCNPs exhibit a low detection sensitivity since they produce luminescence through non-proximity-based re-absorptive energy transfer[38]. It is known that the FRET efficiency is highly dependent on the distance between donors and acceptors[39].

Moreover, viral loads range from $\sim 10^1 - 10^4$ viral copies per μL, translating to ~0.005–5 pM S RBD[40]. 1 mL of S1 protein (10 fg mL^{-1}) corresponds approximately to 1500 viral protein molecules. Remarkably, there is a linear response of S protein from 1 fg mL^{-1} to 16 fg mL^{-1}, and a high concentration at 100 fg mL^{-1}

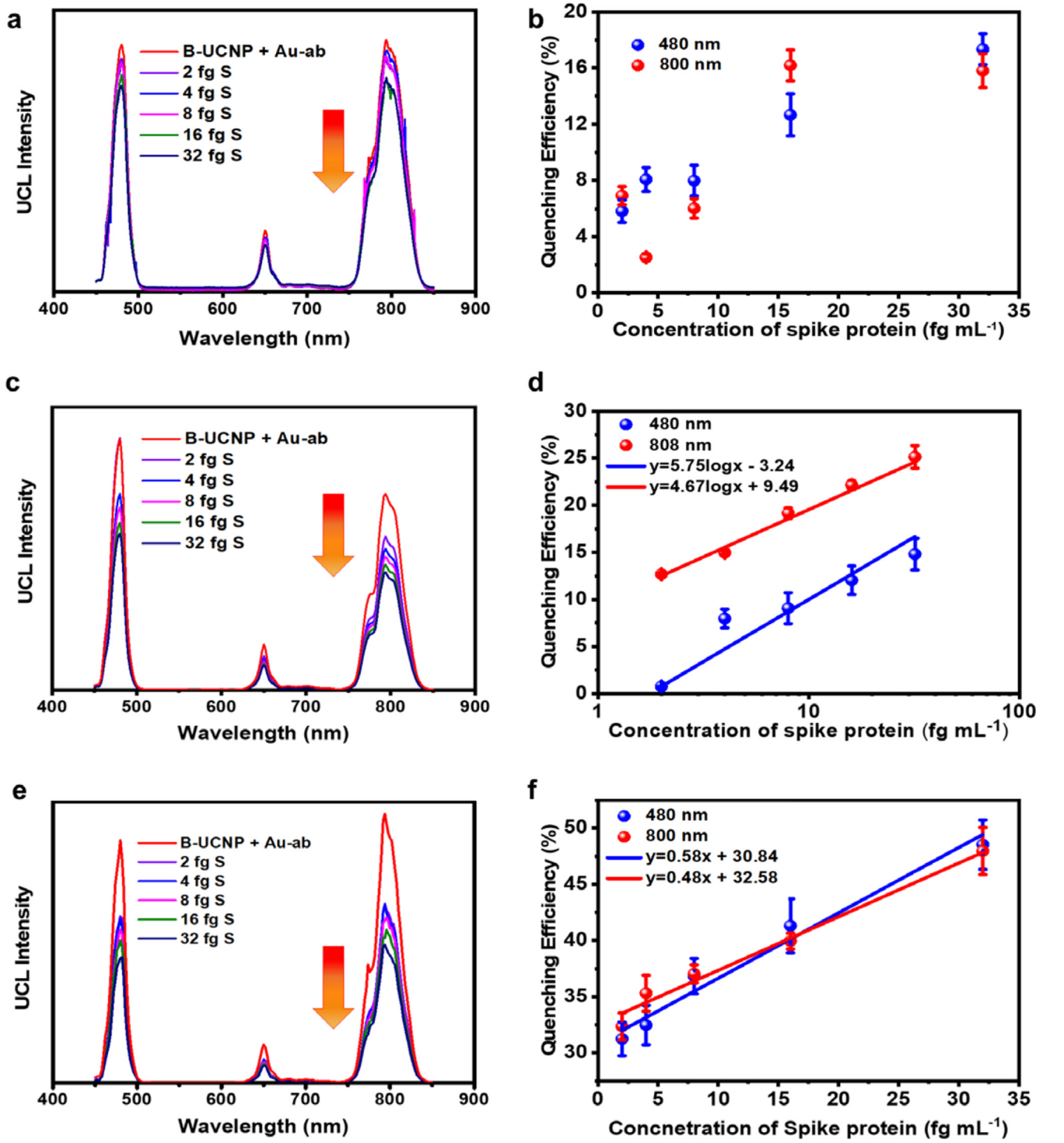

Fig. 3. Optimization of antibody concentrations on AuNRs. UCL spectra of UCNP-Au-abs with **a.** 1 ablod after addition of gradient concentrations of S protein. Quenching efficiency of Au-abs with **b.** 1 ab, **d** 5–6 abs, and **f.** 8–10 abs on B-UCNPs after addition of gradient concentrations of S protein, the results were calculated from a, c and e, respectively.

will cause above 85 % of UCL quenching after co-cultured 90 min at 800 nm. The detected process was repeated for several times and the LOD was calculated as 0.68 fg mL^{-1} after 90 min incubation. Therefore, the lowest detectable concentration at the optimized condition was 0.68 fg mL^{-1}, corresponding to 102 copies of virus. The obtained LOD from our biosensor is much superior to those previously reported carbon nanotubes or graphene-based biosensing platforms for S protein detection[41]. Here, the B-UCNPs with high zeta potential act as both captors and donor in FRET. They capture the free protein in the solution and thus induce a significant improvement in LOD. Table S1 is a comparison between our developed UCNPs-AuNR nanoprobes and other techniques reported so far. Although 980 nm laser diode is essentially utilized in our detection, the NIR laser diode has become portable and cheap nowadays which would facilitate the point-of-care diagnostics. Apparently, our detection exhibited superior advantages compared to most established methods in terms of LOD, consuming time and costs.

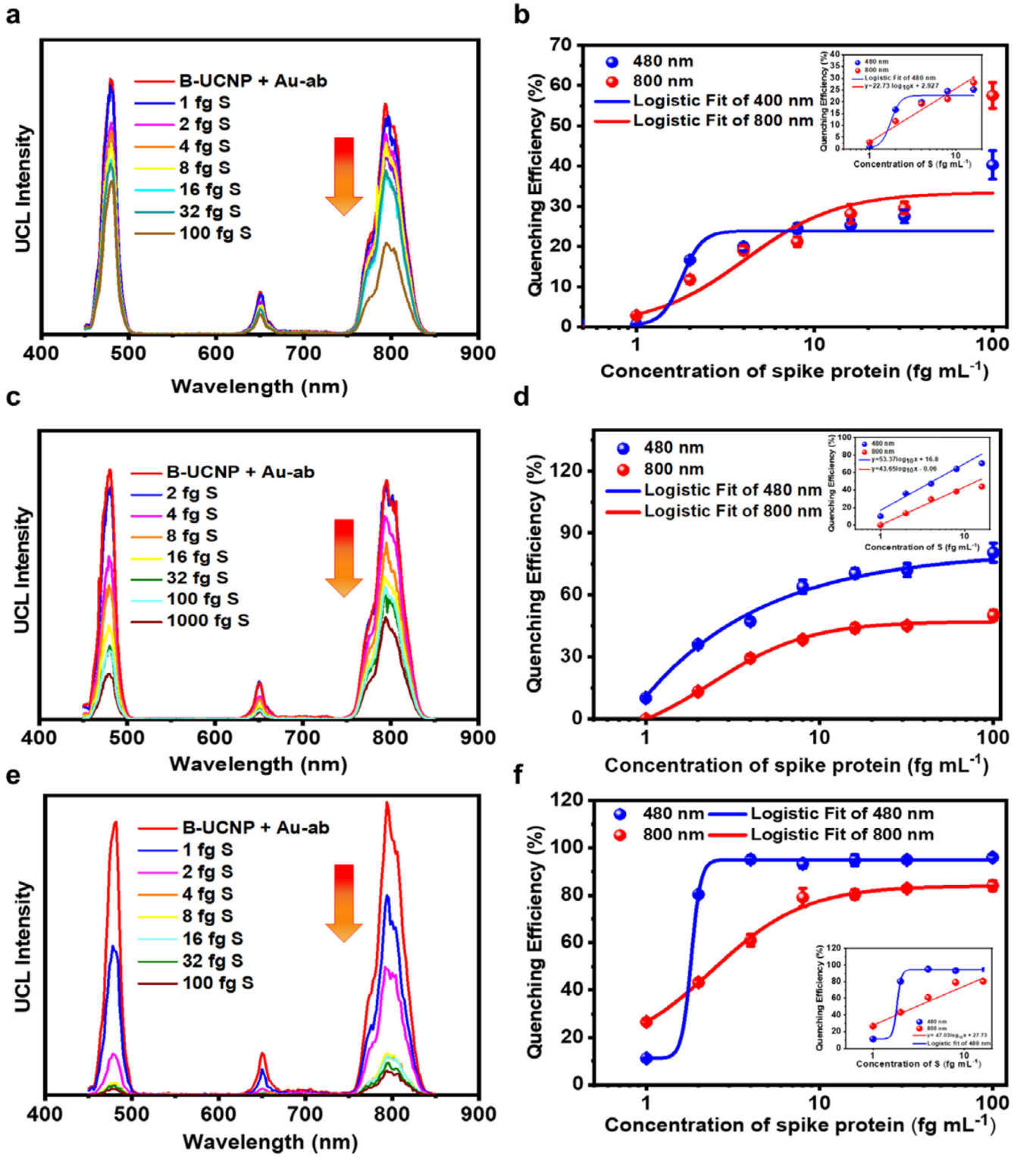

Fig. 4. The effect of incubation time on the detection sensitivity. UCL intensity changes after addition of gradient S protein co-cultured with UCNP-Au abs for **a.** 30 min; **c.** 60 min; **e.** 90 min. Quenching efficiency of UCNP-Au-abs nanosystems after co-cultured with different concentrations of S protein for **b.** 30 min, **d.** 60 min, **f.** 90 min, the results were calculated from **a**, **c** and **e**. The insets are linear/sigmoidal responses of S protein from 1 to 16 fg mL^{-1}.

3.5. The performance of detection under different matrix interference

In principle, the fluorescence-based detection may interfere with various factors, such as buffer, interferents, impurities and various proteins in body fluid in practical applications. It is essential to evaluate the selectivity of the target S spike. As shown in Fig. 5, high concentrations of human serum albumin (HSA) and sialic acid (SA) were added to the detection system (Fig. 5 a, c), they have dramatic influences on the UCL at 480 nm. However, there is a negligible effect on the UCL at 800 nm, illustrating a high stability and reliability in this detection region (Fig. 5 b, d). In addition, we also evaluate the effect of buffers such as lysate and

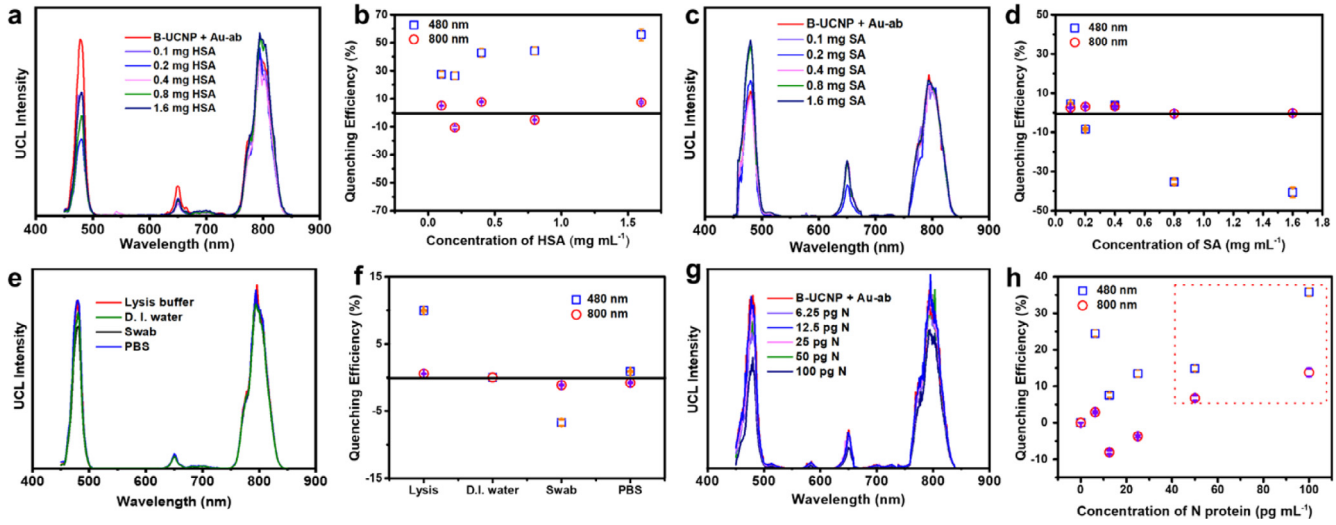

Fig. 5. The UCL changes after incubation with different concentrations of a. HSA (0.1, 0.2, 0.4, 0.8, 1.6 mg mL^{-1}), **c**. SA (0.1, 0.2, 0.4, 0.8, 1.6 mg mL^{-1}), **e.** different buffer solutions and **g.** N protein (6.25, 12.5. 25, 50, 100 pg mL^{-1}). The quenching efficiency of **b**. HSA, **d**. SA, **f.** different buffer solutions and **g.** N protein, the results are calculated from a, c, e, g. The data in the red rectangle of h illustrate the steady detection of N protein from 50 to 100 pg mL^{-1}. (For interpretation of the references to colour in this figure legend, the reader is referred to the web version of this article.)

swabs on the UCL, as expected, swabs and lysis have negligible effect on the detection (Fig. 5 e, f). The selectivity *via* nucleocapsid (N) protein was also assessed, there is negligible changes from 6.25 to 50 pg mL^{-1} at 800 nm. When the concentration of N protein reaches 50 and 100 pg mL^{-1}, a significant UCL decrease could be detected at both 480 nm and 800 nm, which is highlighted by a red rectangle in Fig. 5 g, h. This is because the antibody here has an affinity for N protein. We further compare the N protein detection with commercial test kit, a very shallow test line could be found with 100 pg mL^{-1} N protein in the test strip. Our nanoprobes illustrate a competitive detection method compared with commercial test kits (Fig. S10). Given the growing need for testing, our findings provide support for the high sensitivity detection of S protein and normal detection of N protein, illustrating higher advances than most established method.

3.6. Mechanism of 800 nm detection

To investigate the mechanism of the stable property of detection at the NIR region (800 nm), we study the power dependency of Tm^{3+} and Yb^{3+} co-doped UCNPs. Three-dimensional spectra of Tm^{3+} in the blue region (460–500 nm), the red region (640–

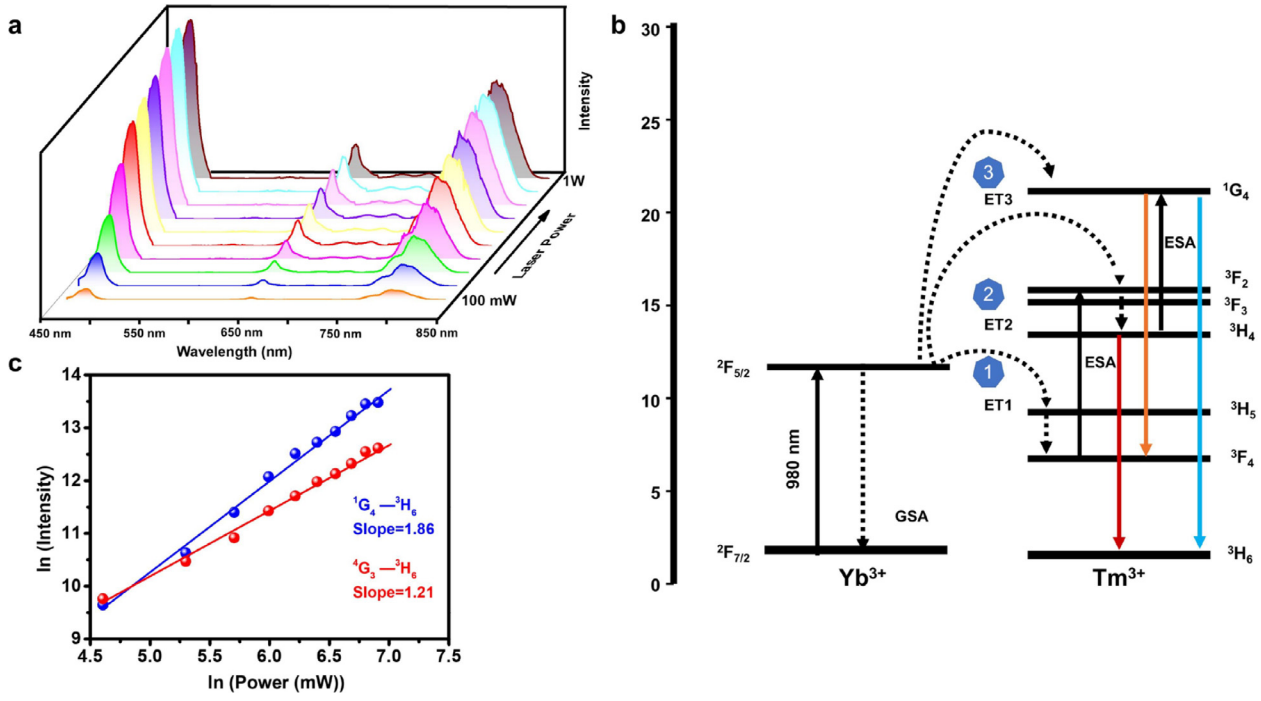

Fig. 6. Power dependence study of $NaYF_4$:Yb/Tm UCNPs. a. The power dependency of UCNPs under 980 nm excitation from 100 mw to 1000 mw. b. The ln (intensity) versus ln (pump power) plots at 480 nm and 800 nm, the blue line and red line represents 480 nm and 800 nm, respectively. C. Mechanism of the Tm^{3+} and Yb^{3+} upconversion process in the UPCNs under 980 nm excitation. (For interpretation of the references to colour in this figure legend, the reader is referred to the web version of this article.)

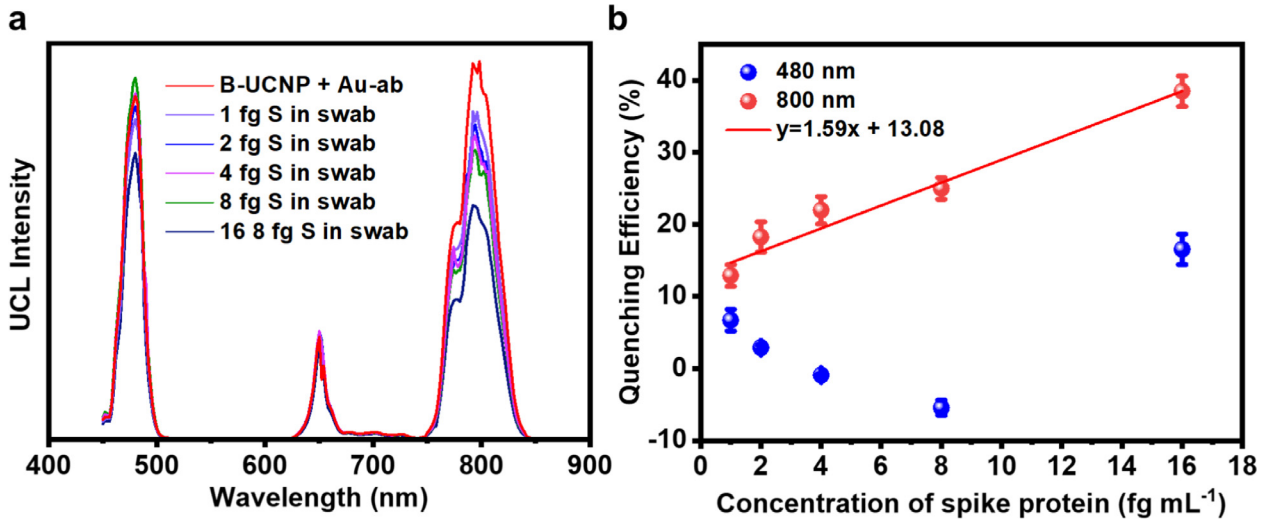

Fig. 7. Detection of S protein in swabs. a. UCL intensity changes with gradient S protein in swabs. **b.** The corresponding UCL quenching efficiency from **a.** The detection process was finished in 5 min with the optimal antibody concentration on AuNRs.

670 nm) and the NIR region (760–830 nm) with different pump power from 100 mW to 1000 mW is shown in Fig. 6a, the emission intensity varies with the pump power, and the increasing trend is different in blue region and NIR region. The three energy transitions of $^1G_4$ to $^3H_6$, $^1G_4$ to $^3F_4$, and $^3H_4$ to $^3H_6$ are corresponding with the emission at 480 nm, red 650 nm and 800 nm (Fig. 6b), respectively. Briefly, ground-state absorption (GSA), excited-state absorption (ESA), energy transfer (ET), and non-radiative relaxation (NR) mainly participate in the upconversion process. For NIR emission in Tm^{3+} and Yb^{3+} co-doped nanocrystals, Yb^{3+} ions are firstly pumped from ground state level $^2F_{7/2}$ to $^2F_{5/2}$ under 980 nm laser, and then transmit to $^3H_5$ level in Tm^{3+} ions through the ET process, and then back to $^3F_4$, after an ESA process ($^3F_4$ to $^3F_2$) and NR ($^3F_2$ to $^3H_4$) process, NIR emission of 800 nm was happened because of the radiative relaxation from $^3H_4$ to $^3H_6$. A total of 5 processes participated in the NIR emission. While for the blue emission process, more complex processes happened, an additional ESA process from excited state $^3H_4$ to $^1G_4$ is needed to ensure the blue emission from $^1G_4$ to the ground state $^3H_6$ (Fig. 6b). Typically, the relationship between pump power (P) and the emission intensity (I) is $P \propto I^n$[42,43], where n is the number of photons in the upconversion process. As can be seen in Fig. 6 c, the probability of energy transfer in the NIR region ($^3H_4$ to $^3H_6$) is higher than in the blue region ($^1G_4$ to $^3H_6$), i.e., the emission at the NIR region plays a dominant role in this upconversion process. Here, 200 mW power was applied to the detection process to ensure sensitivity and avoid the thermal effect. Thus, the emission in the NIR region is steadier than the blue region.

3.7. Detection of S protein in swabs

The collection of saliva samples by patients themselves alleviates demands for supplies of swabs and personal protective equipment. Here, to mimic the clinical detection, we test the S protein in swabs. As shown in Fig. 7 a, b, there is a linear response to different concentration of S protein at 800 nm. By contrast, the response at 480 nm is random and disorganized. Moreover, 10 samples with blind and random concentrations of S protein have further tested for 5 consecutive times, the recoveries and variations (CV%) were shown in Table S2, the recovery rate is between 80 % – 120 %, and the CV% is below 20 %, illustrating the reliability of the detection. Therefore, by virtue of the intriguing merits of high stability, non-autofluorescence and low sample interferents, it is important to note that the detection sensitivity and accuracy are highly dependent on the NIR emission (800 nm) of UCNPs.

4. Conclusions

In summary, we have fabricated a rapid and ultrasensitive FRET-based AuNR-UCNP nanoprobes for spike protein detection. In this work, the B-UCNPs work as captors and donors and AuNRs modified with anti-S antibodies as acceptors. The dedicatedly designed overlap between $NaYF_4$: Yb/Tm and AuNRs reduces the signal-to-noise ratio and improves the sensitivity of the analysis and the limit of detection (LOD). The whole detection process can be completed in minutes after the addition of S protein, with the limit of detection (LOD) 1.06 fg mL^{-1} (~150 copies mL^{-1}). The linear detection range is from 2 fg mL^{-1} to 32 fg mL^{-1}. In addition, this nano biosensing system shows no cross-reactivity to HSA, SA and lysis buffer in the NIR detection (800 nm) band, and we have also illustrated the possible mechanism of the stable property at 800 nm using power-dependency study. Moreover, the nanoprobes show competitive N protein detection capability, which is comparable with commercial test kit. Importantly, the formed AuNR-UCNP core-satellite structure dramatically increased the detection sensitivity. The developed point-of-care diagnostic method based on FRET effect of UCNPs and Au-NRs is capable of detecting COVID-19 virus timely and conveniently, which shed new light on the rapid test and control of the spread of COVID-19. More importantly, this design can be potentially expanded to sensing other related antigen, antibody and protein.

CRediT authorship contribution statement

Lihua Li: Conceptualization, Methodology, Writing – original draft. **Menglin Song and Xinyue Lao:** Methodology, Writing. **Sin-Yi Pang, Yuan Liu and Man-Chung Wong:** Methodology. **Mo Yang:** Review & editing. **Jianhua Hao:** Resources, Conceptualization, Writing – review & editing, Validation, Supervision.

Data availability

Data will be made available on request.

Declaration of Competing Interest

The authors declare that they have no known competing financial interests or personal relationships that could have appeared to influence the work reported in this paper.

Acknowledgements

The work described in this paper was fully supported by a grant from the Research Grants Council of the Hong Kong Special Administrative Region, China (Project No. CRF No. PolyU C5110-20G) and PolyU Internal Research Fund (1-CD4S, 1-W18E).

Appendix A. Supplementary material

Methods, XRD spectra, DLS size, zeta potential, FTIR spectra, UCL emission, absorption spectra, TEM image, UCL changes and photo of test kit. Supplementary data to this article can be found online at https://doi.org/10.1016/j.matdes.2022.111263.

References

[1] C. Huang, Y. Wang, X. Li, L. Ren, J. Zhao, Y. Hu, L. Zhang, G. Fan, J. Xu, X. Gu, Z. Cheng, T. Yu, J. Xia, Y. Wei, W. Wu, X. Xie, W. Yin, H. Li, M. Liu, Y. Xiao, H. Gao, L. Guo, J. Xie, G. Wang, R. Jiang, Z. Gao, Q. Jin, J. Wang, B. Cao, Clinical features of patients infected with 2019 novel coronavirus in Wuhan, China, Lancet 395 (10223) (2020) 497–506.
[2] M. Yüce, E. Filiztekin, K.G. Özkaya, COVID-19 diagnosis—a review of current methods, Biosens. Bioelectron. 172 (2021) 112752.
[3] B. Freire-Paspuel, D. Morales-Jadan, M. Zambrano-Mila, F. Perez, M.A. Garcia-Bereguiain, Analytical sensitivity and clinical performance of" COVID-19 RT-PCR Real TM FAST (CY5)(ATGen, Uruguay) and" ECUGEN SARS-CoV-2 RT-qPCR" (UDLA-STARNEWCORP, Ecuador)": High quality-low cost local SARS-CoV-2 tests for South America, PLOS Neglect. Trop. D. 16 (4) (2022) e0010082.
[4] Y. Wan, C. Zong, X. Li, A. Wang, Y. Li, T. Yang, Q. Bao, M. Dubow, M. Yang, L.-A. Rodrigo, C. Mao, New Insights for Biosensing: Lessons from Microbial Defense Systems, Chem. Rev. (2022).
[5] B. Yin, W.K.H. Ho, Q. Zhang, C. Li, Y. Huang, J. Yan, H. Yang, J. Hao, S.H.D. Wong, M. Yang, Magnetic-Responsive Surface-Enhanced Raman Scattering Platform with Tunable Hot Spot for Ultrasensitive Virus Nucleic Acid Detection, ACS Appl. Mater. Inter. (2022).
[6] L. Ye, X. Xu, S. Song, L. Xu, H. Kuang, C. Xu, Rapid colloidal gold immunochromatographic assay for the detection of SARS-CoV-2 total antibodies after vaccination, J. Mater. Chem. B 10 (11) (2022) 1786–1794.
[7] M. Song, M. Yang, J. Hao, Pathogenic virus detection by optical nanobiosensors, Cell Reports Phys. Sci. (2021) 100288.
[8] K. Jiang, D.S. Jokhun, C.T. Lim, Microfluidic detection of human diseases: From liquid biopsy to COVID-19 diagnosis, J. Biomech. (2021) 110235.
[9] F. Ghorbanizamani, H. Moulahoum, F. Zihnioglu, S. Evran, C. Cicek, R. Sertoz, B. Arda, T. Goksel, K. Turhan, S. Timur, Quantitative paper-based dot blot assay for spike protein detection using fuchsine dye-loaded polymersomes, Biosens. Bioelectron. 192 (2021) 113484.
[10] P.D. Burbelo, F.X. Riedo, C. Morishima, S. Rawlings, D. Smith, S. Das, J.R. Strich, D.S. Chertow, R.T. Davey Jr., J.I. Cohen, Detection of nucleocapsid antibody to SARS-CoV-2 is more sensitive than antibody to spike protein in COVID-19 patients, MedRxiv (2020).
[11] H.A. Alhadrami, A.M. Hassan, R. Chinnappan, H. Al-Hadrami, W.H. Abdulaal, E. I. Azhar, M. Zourob, Peptide substrate screening for the diagnosis of SARS-CoV-2 using fluorescence resonance energy transfer (FRET) assay, Microchim. Acta 188 (4) (2021) 137.
[12] S. Belouzard, J.K. Millet, B.N. Licitra, G.R. Whittaker, Mechanisms of Coronavirus Cell Entry Mediated by the Viral Spike Protein, Viruses 4 (6) (2012) 1011–1033.
[13] Z. Ke, J. Oton, K. Qu, M. Cortese, V. Zila, L. McKeane, T. Nakane, J. Zivanov, C.J. Neufeldt, B. Cerikan, Structures and distributions of SARS-CoV-2 spike proteins on intact virions, Nature 588 (7838) (2020) 498–502.
[14] Y. Liu, D. Tu, H. Zhu, E. Ma, X. Chen, Lanthanide-doped luminescent nano-bioprobes: from fundamentals to biodetection, Nanoscale 5 (4) (2013) 1369–1384.
[15] J. Liao, J. Zhou, Y. Song, B. Liu, Y. Chen, F. Wang, C. Chen, J. Lin, X. Chen, J. Lu, Preselectable optical fingerprints of heterogeneous upconversion nanoparticles, Nano Lett. 21 (18) (2021) 7659–7668.
[16] Y. Kuang, J. Xu, C. Wang, T. Li, S. Gai, F. He, P. Yang, J. Lin, Fine-tuning Ho-based red-upconversion luminescence by altering NaHoF4 core size and NaYbF4 shell thickness, Chem. Mater. 31 (19) (2019) 7898–7909.
[17] B. Gu, Q. Zhang, Recent advances on functionalized upconversion nanoparticles for detection of small molecules and ions in biosystems, Adv. Sci. 5 (3) (2018) 1700609.
[18] M.K. Tsang, W. Ye, G. Wang, J. Li, J. Hao, Ultrasensitive Detection of Ebola Virus Oligonucleotide Based on Upconversion Nanoprobe/Nanoporous Membrane System, ACS Nano 10 (1) (2015) 598.
[19] L. Yang, X. Chen, P. Ma, D. Jin, J. Zhou, H. He, Z. Cheng, J. Lin, Upconversion nanoparticles coated with molecularly imprinted polymers for specific sensing, Dalton Trans. 49 (47) (2020) 17200–17206.
[20] W.W. Ye, M.-K. Tsang, X. Liu, M. Yang, J. Hao, Upconversion Luminescence Resonance Energy Transfer (LRET)-Based Biosensor for Rapid and Ultrasensitive Detection of Avian Influenza Virus H7 Subtype, Small 10 (12) (2014) 2390–2397.
[21] F. Wang, X. Liu, Upconversion multicolor fine-tuning: visible to near-infrared emission from lanthanide-doped NaYF4 nanoparticles, J. Am. Chem. Soc. 130 (17) (2008) 5642–5643.
[22] J. Xu, S. Zhou, D. Tu, W. Zheng, P. Huang, R. Li, Z. Chen, M. Huang, X. Chen, Sub-5 nm lanthanide-doped lutetium oxyfluoride nanoprobes for ultrasensitive detection of prostate specific antigen, Chem. Sci. 7 (4) (2016) 2572–2578.
[23] X. Ye, L. Jin, H. Caglayan, J. Chen, G. Xing, C. Zheng, V. Doan-Nguyen, Y. Kang, N. Engheta, C.R. Kagan, C.B. Murray, Improved Size-Tunable Synthesis of Monodisperse Gold Nanorods through the Use of Aromatic Additives, ACS Nano 6 (3) (2012) 2804–2817.
[24] H.D. Hill, C.A. Mirkin, The bio-barcode assay for the detection of protein and nucleic acid targets using DTT-induced ligand exchange, Nat. Protoc. 1 (1) (2006) 324–336.
[25] X. Wang, Z. Mei, Y. Wang, L. Tang, Comparison of four methods for the biofunctionalization of gold nanorods by the introduction of sulfhydryl groups to antibodies, Beilstein J. Nanotech. 8 (1) (2017) 372–380.
[26] A. Shrivastava, V.B. Gupta, Methods for the determination of limit of detection and limit of quantitation of the analytical methods, Chron. Young Sci. 2 (1) (2011) 21–25.
[27] P. Huang, W. Zheng, S. Zhou, D. Tu, Z. Chen, H. Zhu, R. Li, E. Ma, M. Huang, X. Chen, Lanthanide-doped LiLuF4 upconversion nanoprobes for the detection of disease biomarkers, Angew. Chem. Int. Edit. 126 (5) (2014) 1276–1281.
[28] L. Wightman, R. Kircheis, V. Rossler, S. Carotta, R. Ruzicka, M. Kursa, E. Wagner, Different behavior of branched and linear polyethylenimine for gene delivery in vitro and in vivo, J. Gene Med. 3 (4) (2001) 362–372.
[29] Z. Dai, T. Gjetting, M.A. Mattebjerg, C. Wu, T.L. Andresen, Elucidating the interplay between DNA-condensing and free polycations in gene transfection through a mechanistic study of linear and branched PEI, Biomaterials 32 (33) (2011) 8626–8634.
[30] Z. Li, S. Lv, Y. Wang, S. Chen, Z. Liu, Construction of LRET-Based Nanoprobe Using Upconversion Nanoparticles with Confined Emitters and Bared Surface as Luminophore, J. Am. Chem. Soc. 137 (9) (2015) 3421–3427.
[31] A. Yin, Y. Zhang, L. Sun, C. Yan, Colloidal synthesis and blue based multicolor upconversion emissions of size and composition controlled monodisperse hexagonal NaYF 4: Yb, Tm nanocrystals, Nanoscale 2 (6) (2010) 953–959.
[32] M.K. Tsang, Y.T. Wong, T.H. Tsoi, W.T. Wong, J. Hao, Upconversion Luminescence Sandwich Assay For Detection of Influenza H7 Subtype, Adv. Healthc. Mater. 8 (18) (2019) e1900575.
[33] L. Xu, H. Kuang, C. Xu, W. Ma, L. Wang, N.A. Kotov, Regiospecific plasmonic assemblies for in situ Raman spectroscopy in live cells, J. Am. Chem. Soc. 134 (3) (2012) 1699–1709.
[34] S. Lu, J. Ke, X. Li, D. Tu, X. Chen, Luminescent nano-bioprobes based on NIR dye/lanthanide nanoparticle composites, Aggregate 2 (5) (2021) e59.
[35] Y. Liu, G. Bai, L. Jiang, Y. Hua, L. Chen, S. Xu, Lanthanide Nd ion-doped two-dimensional In2Se3 nanosheets with near-infrared luminescence property, Nanophotonics 9 (8) (2020) 2407–2414.
[36] F. Wang, J. Wang, X. Liu, Direct evidence of a surface quenching effect on size-dependent luminescence of upconversion nanoparticles, Angew. Chem. Int. Edit. 49 (41) (2010) 7456–7460.
[37] R. Huschka, J. Zuloaga, M.W. Knight, L.V. Brown, P. Nordlander, N.J. Halas, Light-Induced Release of DNA from Gold Nanoparticles: Nanoshells and Nanorods, J. Am. Chem. Soc. 133 (31) (2011) 12247–12255.
[38] F. Wang, D. Banerjee, Y. Liu, X. Chen, X. Liu, Upconversion nanoparticles in biological labeling, imaging, and therapy, Analyst 135 (8) (2010) 1839–1854.
[39] J. Shi, F. Tian, J. Lyu, M. Yang, Nanoparticle based fluorescence resonance energy transfer (FRET) for biosensing applications, J. Mater. Chem. B 3 (35) (2015) 6989–7005.
[40] L. Zou, F. Ruan, M. Huang, L. Liang, H. Huang, Z. Hong, J. Yu, M. Kang, Y. Song, J. Xia, SARS-CoV-2 viral load in upper respiratory specimens of infected patients, New Engl. J. Med. 382 (12) (2020) 1177–1179.
[41] R.L. Pinals, F. Ledesma, D. Yang, N. Navarro, S. Jeong, J.E. Pak, L. Kuo, Y.-C. Chuang, Y.-W. Cheng, H.-Y. Sun, M.P. Landry, Rapid SARS-CoV-2 Spike Protein Detection by Carbon Nanotube-Based Near-Infrared Nanosensors, Nano Lett. 21 (5) (2021) 2272–2280.
[42] F. Vetrone, V. Mahalingam, J.A. Capobianco, Near-infrared-to-blue upconversion in colloidal BaYF5: Tm3+, Yb3+ nanocrystals, Chem. Mater. 21 (9) (2009) 1847–1851.
[43] Y. Liu, G. Bai, E. Pan, Y. Hua, L. Chen, S. Xu, Upconversion fluorescence property of Er3+/Yb3+ codoped lanthanum titanate microcrystals for optical thermometry, J. Alloy. Compd. 822 (2020) 153449.